MIT Open Access Articles

Visual Grouping by Neural Oscillator Networks

Massachusetts Institute of Technology

Visual Grouping by Neural Oscillator Networks

Guoshen Yu and Jean-Jacques Slotine

Abstract—**Distributed synchronization is known to occur at several scales in the brain, and has been suggested as playing a key functional role in perceptual grouping. State-of-the-art visual grouping algorithms, however, seem to give comparatively little attention to neural synchronization analogies. Based on the framework of concurrent synchronization of dynamical systems, simple networks of neural oscillators coupled with diffusive connections are proposed to solve visual grouping problems. The key idea is to embed the desired grouping properties in the choice of the diffusive couplings, so that synchronization of oscillators within each group indicates perceptual grouping of the underlying stimulative atoms, while desynchronization between groups corresponds to group segregation. Compared with state-of-the-art approaches, the same algorithm is shown to achieve promising results on several classical visual grouping problems, including point clustering, contour integration, and image segmentation.**

Index Terms—**Grouping, image segmentation, neural oscillator, synchronization, vision.**

I. INTRODUCTION

CONSIDER Fig. 1. Why do we perceive in these visual stimuli a cluster of points, a straight contour, and a river? How is the identification achieved between a subgroup of stimuli and the perceived objects? These classical questions can be addressed from various points of view, physiological, mathematical, and biological.

Many physiological studies, e.g., [14], [22], [27], and [62], have shown evidence of grouping in visual cortex. Gestalt psychology [61], [37], [24], [11] formalizes the laws of visual perception and addresses some grouping principles such as proximity, good continuation, and color constancy, in order to describe the construction of larger groups from atomic local information in the stimuli.

In computer vision, visual grouping has been studied in various mathematical frameworks including graph-based methods [42], [20] and in particular normalized cuts [48], [8], harmonic analysis [35], probabilistic approaches [12], [10], [9], [11], variational formulations [40], [39], [1], Markov random fields [18], statistical techniques [16], [6], [7], [34], [33], among others [52], [43].

In the brain, at a finer level of functional detail, the distributed *synchronization* known to occur at different scales has been proposed as a general functional mechanism for perceptual grouping [4], [49], [60]. In computer vision, however, comparatively little attention has been devoted to exploiting neural-like oscillators in visual grouping. Wang and his colleagues have performed very innovative work using oscillators for image segmentation [51], [56], [57], [32], [5] and have extended the scheme to auditory segregation [2], [54], [55]. They constructed oscillator networks with local excitatory lateral connections and a global inhibitory connection. Adopting similar ideas, Yen and Finkel have simulated facilitatory and inhibitory interactions among oscillators to conduct contour integration [62]. Li has proposed elaborate visual cortex models with oscillators and applied them on lattice drawings segmentation [28]–[31]. Kuzmina and his colleagues [25], [26] have constructed a simple self-organized oscillator coupling model, and applied it on synthetic lattice images as well. Faugeras *et al.* have started studying oscillatory neural mass models in the contexts of natural and machine vision [13].

Inspired by neural synchronization mechanisms in perceptual grouping, this paper proposes a simple and general neural oscillator algorithm for visual grouping, based on diffusive connections and concurrent synchronization [44]. The key idea is to embed the desired grouping properties in the choice of *diffusive couplings* between oscillators, so that the oscillators synchronize if their underlying visual stimulative atoms belong to the same visual group and desynchronize otherwise. A feedback mechanism and a multilayer extension inspired by the hierarchical visual cortex are introduced. The same algorithm is applied to point clustering, contour integration, and image segmentation.

This paper is organized as follows. Section II introduces a basic model of neural oscillators with diffusive coupling connections, and proposes a general visual grouping algorithm. Sections III–V describe in detail the neural oscillator implementation for point clustering, contour integration, and image segmentation and show a number of examples. The results are compared with normalized cuts, a popular computer vision method [48], [8]. Section VI presents brief concluding remarks. As detailed in Section II-F, the method differs from the work of Wang *et al.* [51], [56], [57], [32], [5] in several fundamental aspects, including the synchronization/desynchronization mechanism and the coupling structure.

II. MODEL AND ALGORITHM

The model is a network of neural oscillators coupled with diffusive connections. Each oscillator is associated to an atomic element in the stimuli, for example, a point, an orientation, or a pixel. Without coupling, the oscillators are desynchronized and oscillate in random phases. Under diffusive coupling with
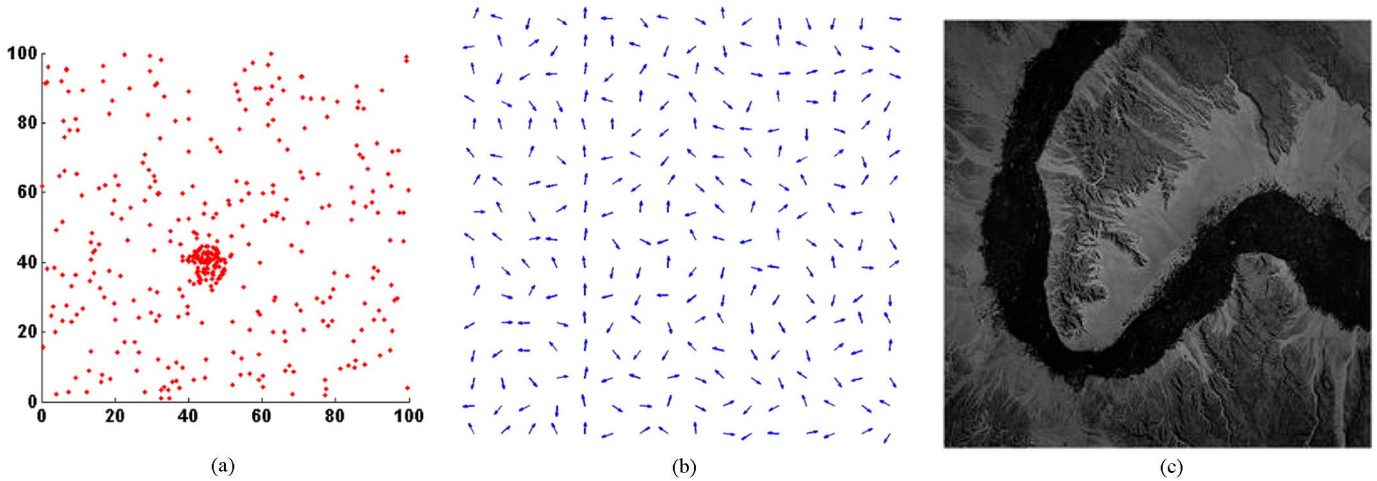
Fig. 1. (a) Cloud of points in which a dense cluster is embedded. (b) Random direction grid in which a vertical contour is embedded. (c) Image in which a river is embedded.
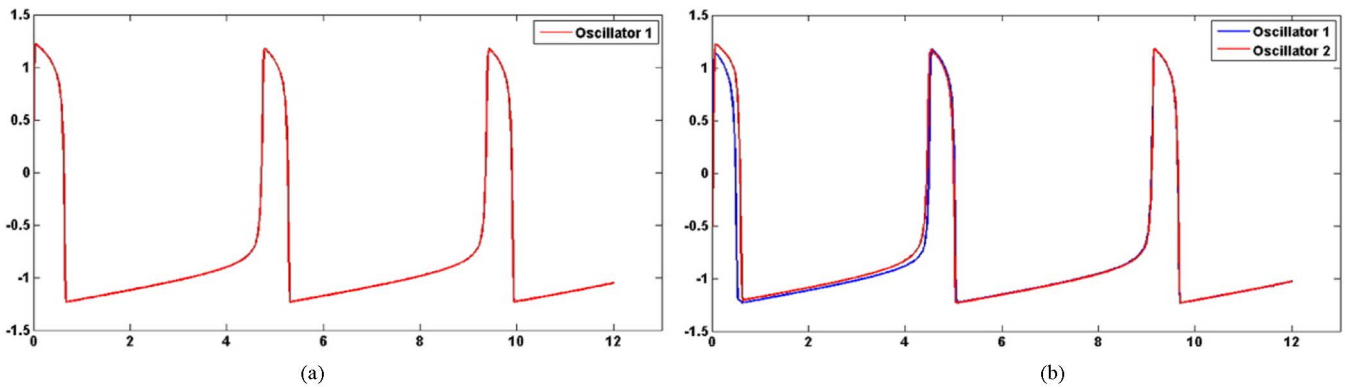

Fig. 2. (a) Oscillation trace of a single oscillator. (b) Synchronization of two oscillators coupled through diffusive connections. The two oscillators start to be fully synchronized at about $t = 5$.

the coupling strength appropriately tuned, they may converge to multiple groups of synchronized elements. The synchronization of oscillators within each group indicates the perceptual grouping of the underlying stimulative atoms, while the desynchronization between groups suggests group segregation.

A. Neural Oscillators

A neural oscillator is an elementary unit associated to an atomic element in the stimuli, and it models the perception of the stimulative atom. We use a modified form of FitzHugh-Nagumo neural oscillators [15], [41], similar to [32], [5]

$$\dot{v}_i = 3v_i - v_i^3 - v_i^7 + 2 - w_i + I_i \qquad (1)$$

$$\dot{w}_i = c[\alpha(1 + \tanh(\rho v_i)) - w_i] \qquad (2)$$

where v_i is the membrane potential of the oscillator, w_i is an internal state variable representing gate voltage, I_i represents the external current input, and α, ρ and c are strictly positive constants. This elementary unit oscillates if I_i exceeds a certain threshold and α, ρ and c are in an appropriate range (within this range, the grouping results have low sensitivities to the values of α, ρ, and c—in all experiments, we use $\alpha = 12, c = 0.04, \rho = 4$). Fig. 2(a) plots the oscillation trace of membrane potential v_i. Other spiking oscillator models can be used similarly.

B. Diffusive Connections

Oscillators are coupled to form a network which aggregates the perception of individual atoms in the visual stimulus. The oscillators are coupled through diffusive connections.

Let us denote by $\mathbf{x_i} = [v_i, w_i]^T$ the state vectors of the oscillators introduced in Section II-A, each with dynamics $\dot{\mathbf{x}}_i = \mathbf{f}(\mathbf{x}_i, t)$. A neural oscillator network is composed of N oscillators, connected with diffusive coupling [58]

$$\dot{\mathbf{x}}_i = \mathbf{f}(\mathbf{x}_i, t) + \sum_{i \neq j} k_{ij}(\mathbf{x}_j - \mathbf{x}_i), \qquad i = 1, \ldots, N \quad (3)$$

where k_{ij} is the coupling strength.

Oscillators i and j are said to be *synchronized* if $\mathbf{x}_i$ remains equal to $\mathbf{x}_j$. Once the elements are synchronized, the coupling terms in (3) disappear, so that each individual element exhibits its natural and uncoupled behavior, as illustrated in Fig. 2. A larger value of k_{ij} tends to reduce the state difference $\mathbf{x}_i - \mathbf{x}_j$ and thus to reinforce the synchronization between oscillators i and j (see the Appendix for more details).

The key to using diffusively coupled neural oscillators for visual grouping is to tune the couplings so that the oscillators synchronize if their underlying atoms belong to the same visual

group, and desynchronize otherwise. According to Gestalt psychology [61], [24], [37], visual stimulative atoms having similarity (e.g., gray level, color, orientation) or proximity tend to be grouped perceptually. This suggests making strong coupling between neural oscillators whose underlying stimuli are similar. Such coupling is implemented by a Gaussian tuning

$$k_{ij} = e^{\frac{-|s_i - s_j|^2}{\beta^2}} \qquad (4)$$

where s_i and s_j are stimuli of the two oscillators, for example, position for point clustering, orientation for contour integration, and gray level for image segmentation; and β is a tuning parameter: the coupling strength falls off as a Gaussian function of the distance between the stimuli. Psychophysical evidence of Gaussian tuning in vision has been observed [45]. In computer vision, Gaussian tuning has been applied in various applications such as image denoising [3], segmentation [48], [43], recognition [47], mean shift clustering [16], [6], [7], and contour integration [62].

C. Generalized Diffusive Connections

The visual cortex is hierarchical. Higher level layers have smaller dimension than lower level layers, as information going from bottom to top turns from redundant to sparse and from concrete to abstract [46], [21]. The presence of extensive anatomical connections between layers, both bottom-up (feedforward) and top-down (feedback), has been well established experimentally [23].

In a hierarchy, generalized diffusive connections between layers can implement consensus between multiple processes of different dimensions [44]. Construction of the hierarchy involves connecting two or more oscillator networks of different sizes. Oscillator networks of sizes N_1 and N_2 can be connected with generalized diffusive connections [59], [44]

$$\dot{\mathbf{x}}_1 = \mathbf{f}_1(\mathbf{x}_1, t) + k_1 \mathbf{A}^T (\mathbf{B}\mathbf{x}_2 - \mathbf{A}\mathbf{x}_1) \qquad (5)$$
$$\dot{\mathbf{x}}_2 = \mathbf{f}_2(\mathbf{x}_2, t) + k_2 \mathbf{B}^T (\mathbf{A}\mathbf{x}_1 - \mathbf{B}\mathbf{x}_2) \qquad (6)$$

where $\mathbf{f}_1$ and $\mathbf{f}_2$ are dynamics of two networks of sizes N_1 and N_2 whose state vectors are, respectively, $\mathbf{x}_1$ and $\mathbf{x}_2$, $\mathbf{A}$ and $\mathbf{B}$ are coupling matrices of appropriate sizes $M \times N_1$ and $M \times N_2$, and k_1 and k_2 are the coupling strengths. The coupling between the two layers is bidirectional if $k_1 \neq 0$ and $k_2 \neq 0$. One-way feedback from top to bottom corresponds to $k_1 \neq 0$ and $k_2 = 0$. The oscillators between the two layers are decoupled if $k_1 = 0$ and $k_2 = 0$. Fig. 3 shows an example of generalized diffusive connection.

For appropriate choices of dynamics, once the two layers are synchronized, i.e., $\mathbf{A}\mathbf{x}_1 = \mathbf{B}\mathbf{x}_2$, the coupling terms disappear, so that each layer exhibits its natural behavior as an independent network, as in the case of diffusive connections.

D. Concurrent Synchronization and Stability

In perception, fully synchronized elements in each group are bound, while different groups are segregated [53]. Concurrent synchronization analysis provides a mathematical tool to study stability and convergence properties of the corresponding neural oscillator networks.
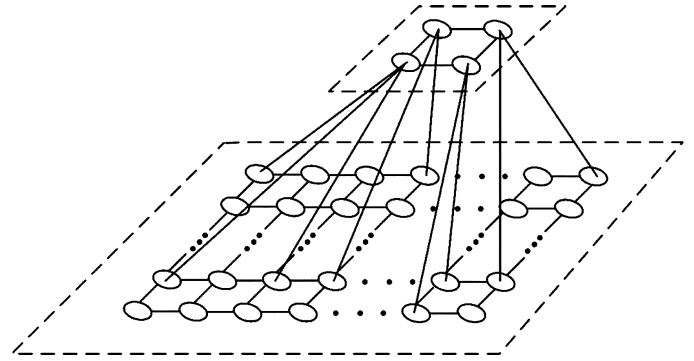

Fig. 3. Two networks (top and bottom) of different dimensions are connected with *generalized diffusive connections* (simplified model of a hierarchical visual cortex with feedforward and feedback connections).

In an ensemble of dynamical elements, *concurrent synchronization* is defined as a regime where the whole system is divided into multiple groups of fully synchronized elements, but elements from different groups are not necessarily synchronized [44]. Networks of oscillators coupled by diffusive connections or generalized diffusive connections defined in Sections II-B and II-C are specific cases of this general framework [44], [58].

A subset of the global state space is called *invariant* if trajectories that start in that subset remain in that subset. In our synchronization context, the invariant subsets of interest are linear subspaces, corresponding to some components of the overall state being equal $(\mathbf{x}_i = \mathbf{x}_j)$ in (3), or verifying some linear relation $(\mathbf{A}\mathbf{x}_1 = \mathbf{B}\mathbf{x}_2)$ in (5) and (6). Concurrent synchronization analysis quantifies stability and convergence to invariant linear subspaces. Furthermore, a property of concurrent synchronization analysis, which turns out to be particularly convenient in the context of grouping, is that the actual invariant subset itself needs not be known *a priori* to guarantee stable convergence to it.

Concurrent synchronization may first be studied in an idealized setting, e.g., with exactly equal inputs to groups of oscillators, and noise-free conditions. This allows one to compute minimum coupling gains to guarantee global exponential convergence to the invariant synchronization subspace. *Robustness* of concurrent synchronization, a consequence of its exponential converge properties, allows the qualitative behavior of the nominal model to be preserved even in nonideal conditions. In particular, it can be shown and quantified that for high convergence rates, actual trajectories differ little from trajectories based on an idealized model [58].

A more specific discussion of stability and convergence is given in the Appendix. The reader is referred to [44] for more details on the analysis tools.

E. Visual Grouping Algorithm

A basic and general visual grouping algorithm is obtained by constructing a neural oscillator network according to the following steps.

1) Construct a neural oscillator network. Each oscillator (1) and (2) is associated to one atom in the stimuli. Oscillators are connected with diffusive connections (3) or generalized
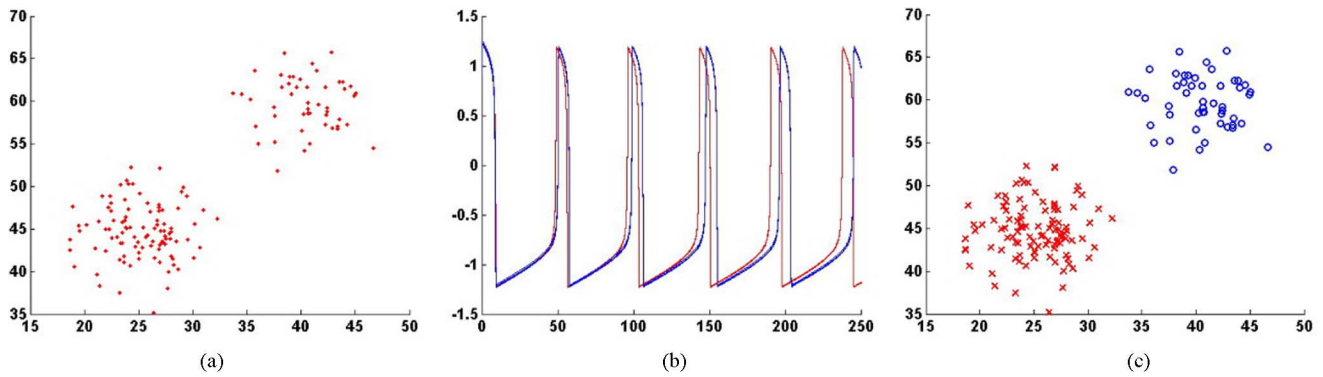
Fig. 4. (a) Points to cluster. (b) Oscillators converge to two concurrently synchronized groups. (c) Clustering results. The circles and the crosses represent the two clusters.
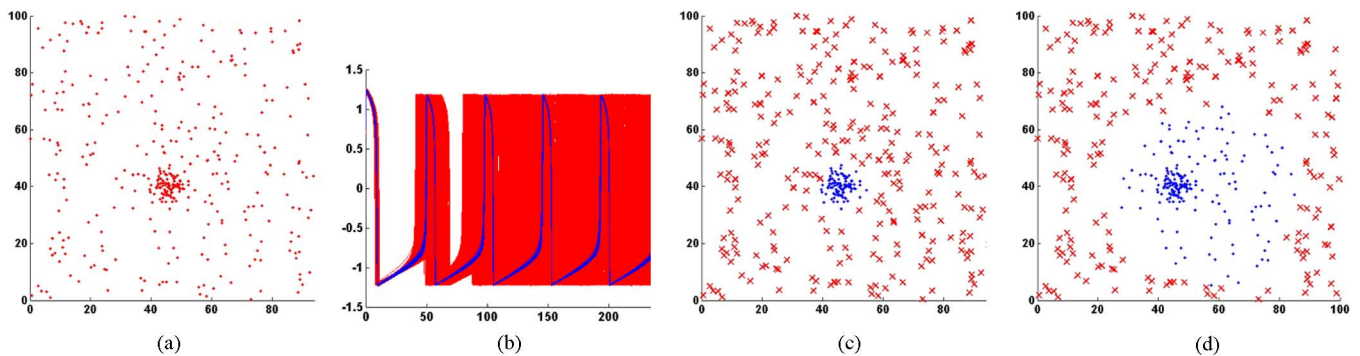

Fig. 5. (a) Cloud of points made of 300 points uniformly randomly distributed in a space of size 100×100, in addition to a cluster of 100 Gaussian distributed points with covariance matrix $[90; 09]$. (b) Neural oscillator system converges to one synchronized group that corresponds to the cluster with all the "outliers" totally desynchronized in the background. (c) and (d) Clustering results by, respectively, neural oscillators and normalized cuts: dots represent the cluster detected by the algorithm and crosses are the "outliers." In the latter many outliers are confused with the cluster of interest.
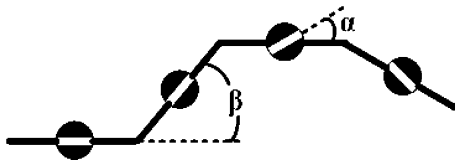

Fig. 6. Element-to-element angle β is the difference in angle of orientation of each successive path segment. The element-to-path angle α is the angle of orientation of the element with respect to the path. This figure is adapted from [14].

diffusive connections (5) and (6) using the Gaussian-tuned gains (4). The coupling tuning for point clustering, contour integration, and image segmentation will be specified in the following sections.

2) Simulate the so-constructed network. The oscillators converge to concurrently synchronized groups.

3) Identify the synchronized oscillators and equivalently the visual groups. A group of synchronized oscillators indicates that the underlying visual stimulative atoms are perceptually grouped. Desynchronization between groups suggests that the underlying stimulative atoms in the two groups are segregated.

The differential equations (1) and (2) are solved using a Runge–Kutta method [with the Matlab ordinary differential equation (ODE) solver]. As a consequence of the global exponential convergence of networks of oscillators coupled by diffusive coupling [58], concurrent synchronization in the neural oscillator networks typically can occur within two or three cycles, and it may be verified by checking the correlation among the traces in potential groups [62]. Fast transients are also consistent with the biological analogy, as in the brain concurrent synchronization is thought to occur transiently over a few oscillation cycles [4]. Once the system converges to the invariant synchronization subspace, synchronization can be identified. As shown in Figs. 4(b) and 5(b), traces of synchronized oscillators coincide in time, while those of desynchronized groups are separated [53]. For point clustering and contour integration, the identification of synchronization in the oscillation traces is implemented by thresholding the correlation among the traces as proposed in [62]. For image segmentation, a k-means algorithm (with random initialization and correlation distance measure) is applied on the oscillation traces to identify the synchronization. A complete description of the basic image segmentation algorithm is given in Fig. 10, which applies to point clustering and contour integration as well. Feedback and multilayer network extensions for image segmentation are detailed in Figs. 14 and 18.

As in most other visual grouping algorithms [48], [7], [43], [62], some parameters, including the number of clusters and a Gaussian tuning parameter, need to be adjusted manually according to the number and size of the groups that one expects to obtain. Automatic parameter selection in visual grouping problems remains an active research topic in computer vision [50]
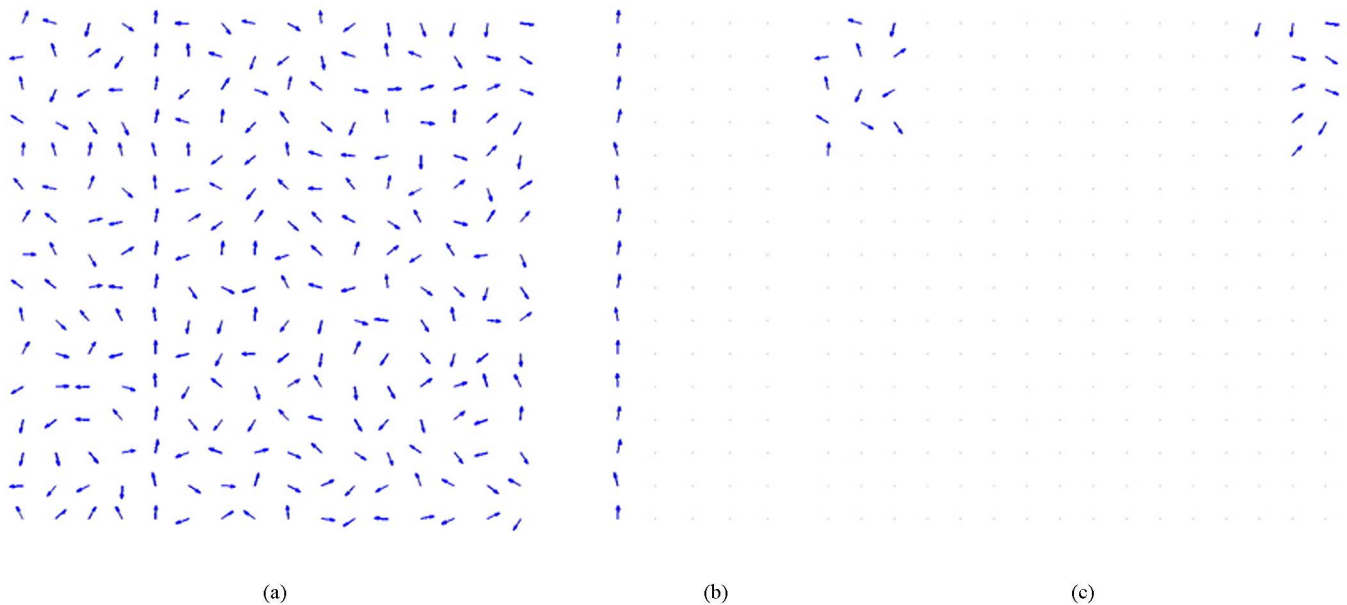
Fig. 7. (a) Vertical contour is embedded in a uniformly distributed orientation grid. (b) and (c) Contour integration by, respectively, neural oscillators and normalized cuts.
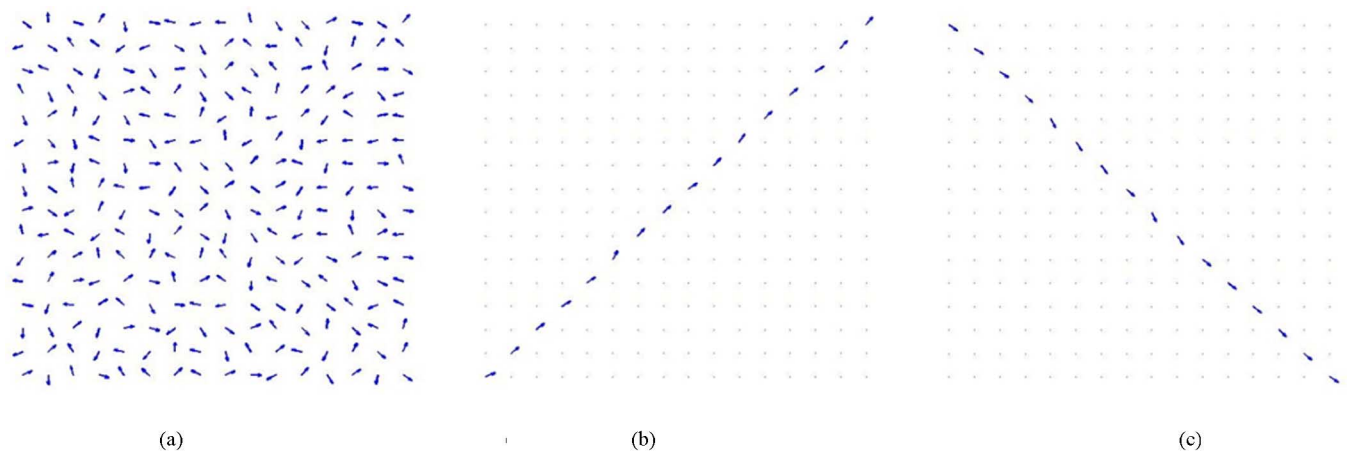

Fig. 8. (a) Two contours are embedded in a uniformly distributed orientation grid. (b) and (c) Two identified contours identified by neural oscillators.

and is out of the scope of this paper which emphasizes neural analogy and implementation.

F. Relation to Previous Work

Among the relatively small body of previous work based on neural oscillators mentioned in Section I, the pioneering work of Wang *et al.* [51], [56], [57], [5] on image segmentation called locally excitatory globally inhibitory oscillator networks (LE-GIONs) is most related to this paper. Yen and Finkel [62] have studied similar ideas for contour integration. While its starting point is the same, namely, achieving grouping through oscillator synchronization and tight coupling between oscillators associated to similar stimuli, the method presented in this paper differs fundamentally from LEGION in the following aspects.

- **Synchronization mechanism**. A global inhibitor that allows active oscillators to inhibit others is a key element in LEGION in order to achieve synchronization within one group and distinction between different groups: at one time only one group of oscillators is active and the others are inhibited. This work relies on *concurrent synchronization*

[44] and does not contain any inhibitor: all oscillators are active simultaneously; multiple groups of oscillators, synchronized within each group and desynchronized between groups, coexist.

- **Coupling mechanism**. The oscillators coupling in LE-GION is obtained through *stimulation*: local excitation coupling is implemented through positive stimulation which tends to activate the oscillators in the neighborhood; global inhibition is obtained by negative stimulation which tends to deactivate other oscillators. The coupling in this work is based on *diffusive* connections (3): the coupling term is a state difference which tends to zero as synchronization occurs [58].

- **Robustness**. The original LEGION was shown to be sensitive to noise [51], [56]. A concept of lateral potential for each oscillator was introduced in a later version of LEGION [57], [5] to improve its robustness and reduce oversegmentation in real image applications. The proposed method based on nonlocal diffusive connections has inherent robustness to noise.
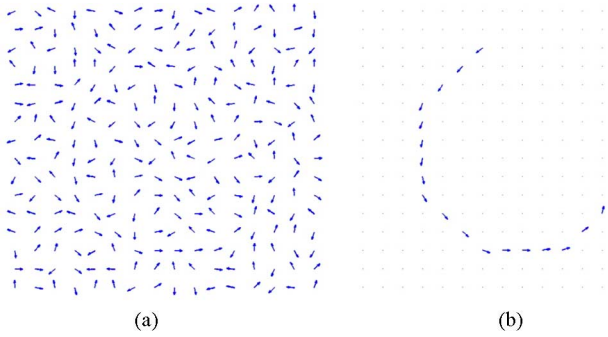
Fig. 9. (a) Smooth curve is embedded in a uniformly distributed orientation grid. (b) Curve identified by neural oscillators.

In turn, these fundamental differences make the proposed neural oscillator framework fairly simple and general. It provides solutions not only for image segmentation, but also for point clustering and contour integration, as detailed in the following sections.

III. POINT CLUSTERING

Point clustering with neural oscillators is based on diffusive connections (3) and follows directly the general algorithm in Section II-E. Let us denote $\mathbf{c}_i = (i_x, i_y)$ the coordinates of a point $\mathbf{p}_i$. Each point $\mathbf{p}_i$ is associated to an oscillator $\mathbf{x}_i$. The proximity Gestalt principle [61], [24], [37] suggests strong coupling between oscillators corresponding to proximate points. More precisely, the coupling strength between $\mathbf{x}_i$ and $\mathbf{x}_j$ is

$$k_{ij} = \begin{cases} e^{\frac{-|\mathbf{c}_i - \mathbf{c}_j|^2}{\beta^2}}, & \text{if } j \in \mathcal{N}_i \\ 0, & \text{otherwise} \end{cases} \qquad (7)$$

where $\mathcal{N}_i$ is the set of M points closest to $\mathbf{p}_i$: an oscillator $\mathbf{x}_i$ is coupled with its M nearest neighbors. Oscillators may be indirectly coupled over larger distances through synchronization propagation (e.g., if $\mathbf{x}_1$ is coupled with $\mathbf{x}_2$ and $\mathbf{x}_2$ is coupled with $\mathbf{x}_3$, then $\mathbf{x}_1$ is indirectly coupled with $\mathbf{x}_3$). β is the main parameter which tunes the coupling. It is adjusted according to the size of the clusters one expects to detect, with a larger β tending to result in bigger clusters. M is a more minor regularization parameter, and the clustering has low sensitivity to M once it is larger than 5. In the experiments, the parameters are configured as $\beta = 3$ and $M = 10$. The external inputs I_i of the oscillators in (1) are chosen as uniformly distributed random variables in the appropriate range.

Fig. 4 illustrates an example in which the points make clearly two clusters (Gaussian distributed, centered at $(25, 40)$ and $(40, 60)$ with covariance matrix $\begin{bmatrix} 9 & 0 \\ 0 & 9 \end{bmatrix}$). As shown in Fig. 4(b), the oscillator system converges to two concurrently synchronized groups separated in the time dimension, each corresponding to one cluster. The identification of the two groups induces the clustering of the underlying points, as shown in Fig. 4(c).

Fig. 5 presents a more challenging setting where one seeks to identify a dense cluster in a cloud of points. The cloud is made

of 300 points uniformly randomly distributed in a space of size 100×100, in addition to a cluster of 100 Gaussian distributed points with covariance matrix $\begin{bmatrix} 9 & 0 \\ 0 & 9 \end{bmatrix}$. The neural oscillator system converges to one synchronized group that corresponds to the cluster with all the "outliers" totally desynchronized in the background, as shown in Fig. 5(b). As in [62], the synchronized traces are segregated from the background by thresholding the correlation among all the traces, which results in the identification of the underlying cluster as shown in Fig. 5(c). The correlation threshold is slightly below 1 in order to have some tolerance to imperfect synchronization and to exclude outliers at the same time. The grouping results have low sensitivity to the correlation threshold once its value is above 0.95. In the experiments, the threshold is set equal to 0.99. The result of normalized cuts [48] is shown in Fig. 5(d): a large number of outliers around the cluster of interest are confused with the cluster.

In this experiment, the neural oscillator solution implemented with Matlab on a Pentium 4 PC takes about 10 s.

IV. CONTOUR INTEGRATION

Field *et al.* [14] have performed interesting experiments to test human capacity of contour integration, i.e., of identifying a path within a field of randomly oriented Gabor elements. They made some quantitative observations in accordance with the Gestalt "good continuation" law [61], [62].

- Contour integration can be made when the successive elements in the path, i.e., the element-to-element angle β (see Fig. 6), differ by $60°$ or less.
- There is a constraint between the element-to-element angle β and the element-to-path angle α (see Fig. 6). The visual system can integrate large differences in element-to-element orientation only when those differences lie along a smooth path, i.e., only when the element-to-path angle α is small enough. For example, with $\alpha = 15°$ and $\beta = 0°$, the contour integration is difficult, even though the observers can easily track a $15°$ orientation difference when there is no variation ($\alpha = 0°$ and $\beta = 15°$).

Figs. 7–9 show the setting of our contour integration experiments, similar to that in [14]. An orientation value $\mathbf{o}_i \in [0, 2\pi)$ is defined for each point $i = (i_x, i_y)$ in a grid, as illustrated by the arrows. Smooth contours potentially imbedded in the grid are to be detected.

Following the general visual grouping algorithm described in Section II-E, neural oscillators with diffusive connections (3) are used to perform contour integration. Each orientation in the grid is associated to one oscillator. The coupling of the oscillators i and j follows the Gestalt law of "good continuation" and, in particular, the results of the psychovisual experiments of [14]

$$k_{ij} = \begin{cases} \exp\left(-\frac{|\mathbf{o}_i - \mathbf{o}_j|^2}{\delta^2} - \frac{\left| \frac{\mathbf{o}_i + \mathbf{o}_j}{2} - \mathbf{o}_{ij} \right|^2}{\gamma^2} \right), & \text{if } |i - j| \leq w \\ 0, & \text{otherwise.} \end{cases} \qquad (8)$$

> **Basic image segmentation.**
>
> 1. Construct the neural oscillator network.
>
>   (a) Make N neural oscillators $\mathbf{x}_i = [v_i, w_i]^T$ following (1,2): $\alpha = 12$, $c = 0.04$, $\rho = 4$, $I_i = a(u_i)$, where u_i is the gray level (0-255) of pixel i, $i = 1, \ldots, N$, with N the number of pixels in the image, and $a(u_i) = (u_i - u_{\min})\frac{I_{\max} - I_{\min}}{u_{\max} - u_{\min}} + I_{\min}$ is an affine mapping that maps the gray level the appropriate external input range $[I_{\min}, I_{\max}]$, with $u_{\min} = \min_i u_i$ and $u_{\min} = \max_i u_i$, $I_{\min} = 0.8$ and $I_{\max} = 2$.
>
>   (b) Couple the N oscillators with diffusive connections (3), where the coupling strength k_{ij} follows the non-local Gaussian tuning (9). The coupling is stronger with bigger β and w. Typical parameter configuration is: $\beta = 20$ for real images, $\beta = \sigma$ for synthetic images contaminated by white Gaussian noise of standard deviation σ; $w = 3$ for images with little or moderate noise, $w = 5$ for very noisy images.
>
> 2. Simulate the neural network by solving the differential equation system constructed in Step 1. In the experiments, the Matlab ODE solver is used to solve the differential equations. Typically the simulation is performed for 6 oscillation cycles and the oscillators converge within 2 or 3 cycles.
>
> 3. Apply a k-means algorithm (with random initialization and correlation distance measure) on the oscillation traces starting from the 3rd cycle after which the oscillators have typically converged. The oscillation traces are clustered in M classes, the corresponding oscillators and underlying pixels follow the same classification.

Fig. 10. Complete algorithm description: basic image segmentation.
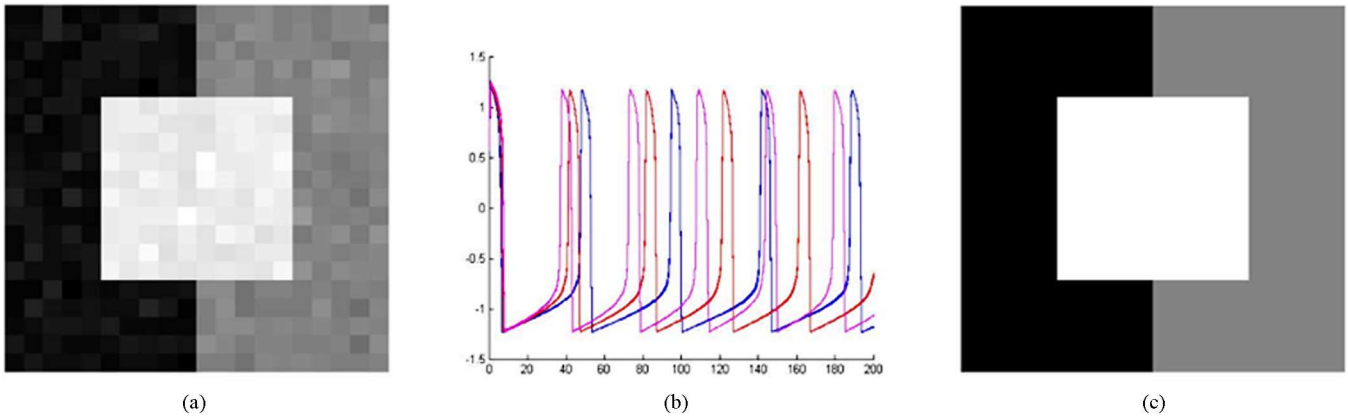
Fig. 11. (a) Synthetic image (the gray levels of the black, gray, and white parts are, respectively, 0, 128, and 255) contaminated by white Gaussian noise of standard deviation $\sigma = 10$. (b) Traces of the neural oscillation ($\beta = \sigma, w = 3$). The oscillators converge into three concurrently synchronized groups. (c) Segmentation in three classes.

where

$$\mathbf{o}_{ij} = \begin{cases} \theta_{ij}, & \text{if } \left| \theta_{ij} - \frac{|\mathbf{o_i} + \mathbf{o_j}|}{2} \right| < \left| \theta_{ij} + \pi - \frac{|\mathbf{o_i} + \mathbf{o_j}|}{2} \right| \\ \theta_{ij} + \pi, & \text{otherwise} \end{cases}$$

is the undirectional orientation of the path ij (the closest to the average element-to-element orientation $|\mathbf{o_i} + \mathbf{o_j}|/2$ modulo π), with $\theta_{ij} = \arctan((i_y - j_y)/(i_x - j_x))$. Oscillators with small element-to-element angle β [the first term in (8)] and small element-to-path angle α [the second term in (8)] are coupled more

tightly. The neural oscillator system makes, therefore, smooth contour integration. δ and γ tune the smoothness of the detected contour. As contour integration is known to be rather local [14], the coupling (8) is effective within a neighborhood of size $(2w+1) \times (2w+1)$. In the experiments, the parameters are configured as $\delta = 20°, \gamma = 10°$, and $w = 1$, in line with the results of the psychovisual experiments of Field *et al.* [14]. The external inputs I_i of the oscillators in (1) are set proportional to the underlying orientations $\mathbf{o}_i$.

Fig. 7(a) presents a grid in which orientations are uniformly distributed in space, except for one vertical contour. The orien-
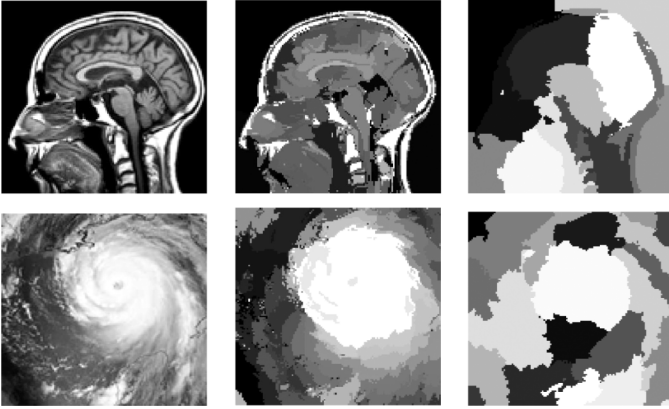
Fig. 12. Real image segmentation. From top to bottom, left to right: a sagittal MRI image (128×128); segmentation in 15 classes by neural oscillators and multiscale normalized cuts; a radar image (128×128); segmentation in 20 classes by neural oscillators and multiscale normalized cuts. Neural oscillator network is configured with $\beta = 20$ and $w = 3$.

tation of the elements on the vertical contour undertakes furthermore a Gaussian perturbation of standard deviation $\sigma = 10°$. The neural oscillator system converges to one synchronized group that corresponds to the contour with all the other oscillators desynchronized [the traces are similar to Fig. 5(b)]. As in [62], the synchronized group is segregated from the background by thresholding the correlation among the traces. As in point clustering, the correlation threshold is slightly below 1 in order to have some tolerance to imperfect synchronization and to exclude outliers at the same time. The grouping results have low sensitivity to the correlation threshold once its value is above 0.95. In the experiments, the threshold is set equal to 0.99. This results in the "pop-out" of the contour shown in Fig. 7(b). As shown in Fig. 7(c), the multiscale normalized cut [8] does not succeed to segregate the contour from the background. (Normalized cuts fail in the following contour integration experiments as well and are not shown.) Fig. 8 illustrates a similar example with two intersecting straight contours.

Fig. 9(a) illustrates a smooth curve embedded in the uniformly randomly distributed orientation background. With some minor effort, subjects are able to identify the curve due to its "good continuation." Similarly, the neural system segregates the curve from the background with the oscillators lying on the curve fully synchronized, as illustrated in Fig. 9(b).

In these experiment, the neural oscillator solution implemented with Matlab on a Pentium 4 PC takes about 10 s.

V. IMAGE SEGMENTATION

The proposed image segmentation scheme follows the general visual grouping algorithm described in Section II-E. In addition to the basic image segmentation, two hierarchical oscillator network extensions are introduced: a feedback mechanism incorporates an image regularity prior that improves the image segmentation under very strong noise perturbation; a multilayer network inspired by the hierarchical visual cortex segments the images pyramidally and provides a faster segmentation solution on large images.
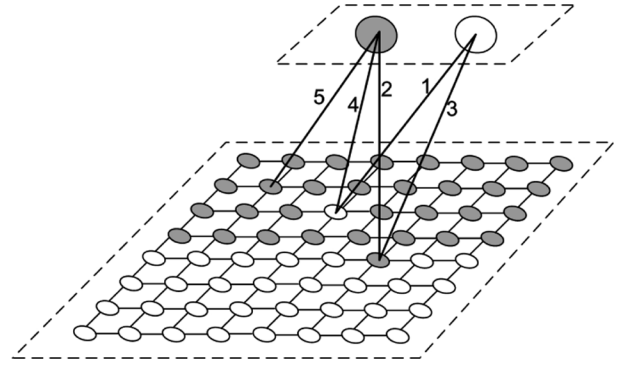

Fig. 13. Neural network with feedback for image segmentation. In the first layer, one oscillator is associated to each pixel. An oscillator is coupled within all the others in a neighborhood of size $(2w + 1) \times (2w + 1)$ (for clarity only couplings with the four nearest neighbors are shown in the figure). The image is segmented into two regions marked by white and gray. The second layer contains two oscillators, each representing a class previously segmented with the external input equal to the average gray level of that class. The coupling strength between an oscillator indexed by the coordinates (i_x, i_y) in the first layer and an oscillator indexed by the regions $m = 1, 2$ in the second layer is proportional to number of the pixels in the neighborhood $\mathcal{N}(i_x, i_y) = \{(i_x, i_y), (i_x \pm 1, i_y), (i_x, i_y \pm 1)\}$ that belong to the region m according to the previous segmentation. Only five such couplings and their strengths are shown for clarity.

A. Basic Image Segmentation

One oscillator is associated to each pixel in the image. Within a neighborhood the oscillators are nonlocally coupled with a coupling strength

$$k_{ij} = \begin{cases} e^{\frac{-|u_i - u_j|^2}{\beta^2}}, & \text{if } |i - j| < w \\ 0, & \text{otherwise} \end{cases} \qquad (9)$$

where $u_\mathbf{i}$ is the pixel gray level at coordinates $i = (i_x, i_y)$ and w adjusts the size of the neighborhood. Pixels with similar gray levels are coupled more tightly, as suggested by the color constancy Gestalt law [61], [24], [37]. As in [62] and [3], a Gaussian function of gray-level difference is used to tune the coupling strength. Nonlocal coupling plays an important role in regularizing the image segmentation, with a larger w resulting in more regularized segmentation and higher robustness to noise. A complete basic image segmentation algorithm description is given in Fig. 10.

Fig. 11(a) illustrates a synthetic image (the gray levels of the black, gray, and white parts are 0, 128, and 255) contaminated by white Gaussian noise of moderate standard deviation $\sigma = 10$. The segmentation algorithm was configured with $\beta = \sigma$ and $w = 3$. The external inputs I_i of the oscillators in (1) are set proportional to the underlying gray level u_i. The oscillators converge into three concurrently synchronized groups as plotted in Fig. 11(b), which results in a perfect segmentation as shown in Fig. 11(c). K-means with a random initialization and a correlation distance measure is applied to detect oscillator synchronization in all the image segmentation experiments.

Fig. 12 shows some real image segmentation examples in comparison with the multiscale normalized cuts [8]. Both methods obtain rather regular segmentation with hardly any "salt and pepper" holes. Using the same number of classes, the segmentation obtained by neural oscillators seems more

Image segmentation with feedback.

1. Pre-segment the image to M classes using the basic image segmentation algorithm in Fig. 10. The neural oscillator associated to the pixel (i_x, i_y) constructed on this first-layer is denoted as $\mathbf{x}_1(i_x, i_y)$.

2. Construct (or update) two-layer oscillator network with feedback.

    (a) Make the second-layer network with M neural oscillators $\mathbf{x}_2(m)$, $m = 1, \ldots, M$ (see Step 1-(a) in Fig. 10). Each oscillator represents a class previously segmented. The external input $I_m = a\left(\frac{\sum_{(i_x,i_y)\in \mathcal{C}_m} u_{(i_x,i_y)}}{|\mathcal{C}_m|}\right)$ is the average gray level of class m projected to the appropriate range (see Step 1 in Fig. 10).

    (b) Establish the feedback by coupling the second-layer oscillators $\mathbf{x}_2(m)$ with the first-layer ones $\mathbf{x}_1(i_x, i_y)$ with generalized diffusive connections (5,6). The coupling matrices $\mathbf{A}_{MN \times N}$ and $\mathbf{B}_{MN \times M}$ are designed so that the coupling strength between $\mathbf{x}_2(m)$ and $\mathbf{x}_1(i_x, i_y)$ is equal to the number of pixels in a neighborhood of (i_x, i_y) that belong to class m. An equivalent implementation of the inter-layer coupling is applied in the experiments by considering the two layers as a whole network (3), in which the coupling strength between $\mathbf{x}_2(m)$ and $\mathbf{x}_1(i_x, i_y)$ is defined as $k_{m,(i_x,i_y)} = \delta_{(i_x,i_y)\in \mathcal{C}_m} + \delta_{(i_x-1,i_y)\in \mathcal{C}_m} + \delta_{(i_x+1,i_y)\in \mathcal{C}_m} + \delta_{(i_x,i_y-1)\in \mathcal{C}_m} + \delta_{(i_x,i_y+1)\in \mathcal{C}_m}$, where $\delta_A = 1$ if A is true and 0 otherwise. Since the feedback descends one-way from the second layer to the first, the coupling term $k_{m,(i_x,i_y)}(\mathbf{x}_2(m) - \mathbf{x}_1(i,j))$ in (3) is only added on the first-layer oscillators $\mathbf{x}_1(i_x, i_y)$. This is equivalent to setting $k_1 = 1$ and $k_2 = 0$ in (5,6).

3. Update the segmentation using the oscillator network with feedback constructed in Step 2. The segmentation procedure follows Steps 2 and 3 in the basic image segmentation algorithm in Fig. 10.

4. If the segmentation result does not converge, go to Step 2. Typically the segmentation converges in 10 oscillation cycles in total.

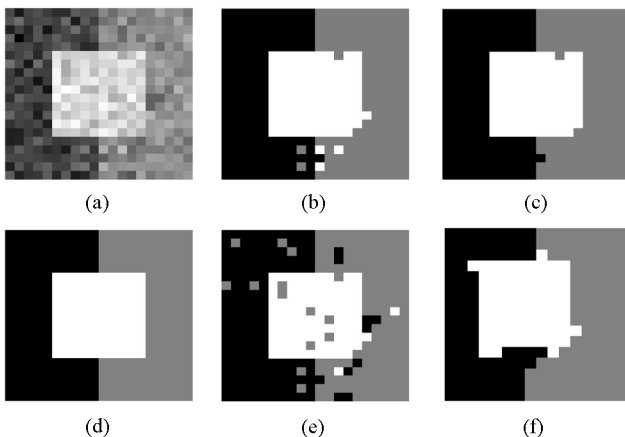Fig. 14. Complete algorithm description: image segmentation with feedback.

Fig. 15. (a) Synthetic image (the gray levels of the black, gray, and white parts are, respectively, 0, 128, and 255) contaminated by white Gaussian noise of standard deviation $\sigma = 40$. (b)–(d) Segmentation by neural oscillators with feedback ($\beta = \sigma$, $w = 5$), shown at the second, fourth, and tenth oscillation cycles. (e) and (f) Segmentation by k-means and multiscale normalized cuts.

accuracy; in the radar image, the cloud boundaries and eye of the hurricane are more precisely segregated.

B. Noisy Image Segmentation With Feedback

Fig. 15(a) shows a synthetic image contaminated by strong white Gaussian noise of standard deviation $\sigma = 40$. Thanks to the nonlocal coupling, the neural oscillator network is robust and segmentation result [Fig. 15(b)] is more regular than those of the algorithms which do not take into account the image regularity prior, such as, e.g., k-means [Fig. 15(e)]. However, due to the heavy noise perturbation, the segmentation result is not perfect. A feedback scheme is introduced to overcome this problem. Specifically, in a loose analogy with the visual cortex hierarchy, a second layer with feedback connections to the first layer is introduced to incorporate prior knowledge, in this case image regularity, i.e., that proximate pixels of natural images are likely to belong to the same region. Feedback from the second layer to the first exploits this regularity to improve the segmentation.

The feedback error correction is implemented using the generalized diffusive connections (5) and (6). On top of the first layer previously described, a second layer of oscillators is added

subtle and closer to human perception: in the sagittal magnetic resonance imaging (MRI), salient regions such as cortex, cerebellum, and lateral ventricle are segregated with good
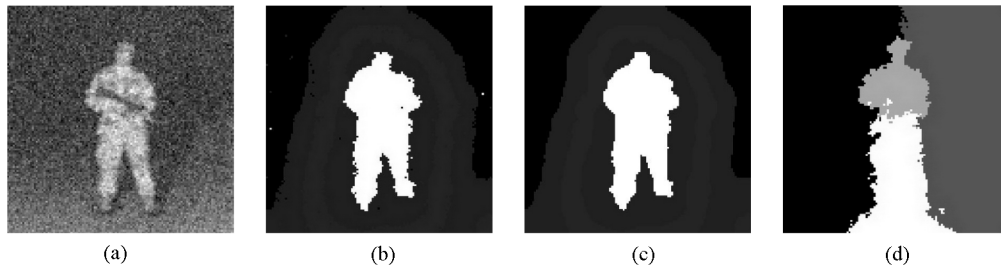
Fig. 16. (a) Infrared image. (b) Segmentation by neural oscillators without feedback ($\beta = 30, w = 5$). (c) Segmentation by neural oscillators with feedback ($\beta = 30, w = 5$). (d) Segmentation by multiscale normalized cuts. The number of classes is four for all the methods.
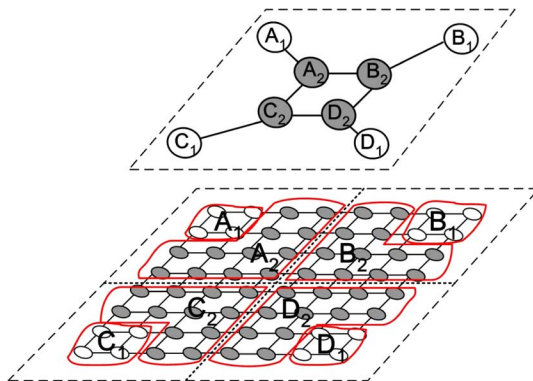

Fig. 17. Two-layer image segmentation. In the first layer, the image is decomposed into four disjoint parts. Each part is segmented using the basic image segmentation algorithm. In the second layer, one oscillator represents a class segmented in the first layer, with the external input equal to the average gray level in that class. Second-layer oscillators whose underlying regions in the first layer are in vicinity are coupled.

and coupled with the first, as shown in Fig. 13. The second layer contains M oscillators, where M is the number of regions obtained in the first layer. Each oscillator represents a class previously segmented with the external input equal to the average gray level of the class. Every oscillator in the first layer, indexed by (i_x, i_y), is coupled with all the M oscillators in the second layer, with the coupling strengths depending on the segmentation obtained in a neighborhood of (i_x, i_y). More precisely, the coupling matrices $\mathbf{A}$ and $\mathbf{B}$ in the generalized diffusive connection (5) and (6) are designed so that the coupling strength from an oscillator $\mathbf{x}_2(m), m = 1, \ldots, M$, in the second layer to an oscillator $\mathbf{x}_1(i_x, i_y)$ in the first layer is proportional to number of pixels in the neighborhood $\mathcal{N}(i_x, i_y)$, which belong to the region m according to the current segmentation—as illustrated in Fig. 13. This interlayer connection reinforces the coupling between the first-layer oscillators and the second-layer ones corresponding to the locally dominant regions, and thus regularizes the segmentation.

For example, in Fig. 13, the misclassified "white" oscillator isolated in the "gray" region on the first layer is now coupled to the second-layer "gray" oscillator with a coupling strength 4 that is much higher than its coupling strength 1 to the second-layer "white" oscillator. Thus, the misclassification is expected to be corrected. After each step of $\mathbf{A}$ and $\mathbf{B}$ adjustment according to the previous segmentation, the oscillator network converges to a new concurrently synchronized status and the segmentation is

updated. Fig. 14 gives a complete algorithm description of the image segmentation with feedback.

Fig. 15(b)–(d) shows the segmentation results at the beginning of the second, fourth, and tenth oscillation cycles. The segmentation errors are corrected as the feedback is going along. The segmentation is stable at Fig. 15(d) after the tenth cycle. Normalized cuts achieves regular segmentation, as shown in Fig. 15(f), but it confuses the regions under the strong noise perturbation.

Fig. 16 illustrates the segmentation of an infrared night vision image heavily noised. The segmentation result of the basic neural oscillators algorithm without feedback contains a few punctual errors and, more importantly, the contour of the segmented object zigzags due to the strong noise perturbation. The feedback procedure corrects the punctual errors and regularizes the contour. The normalized cuts segmentation results in highly irregular contours and confuses the lower part of the solder with the background.

C. Multilayer Image Segmentation

Multilayer oscillator networks imitate the hierarchical structure of the cortex, where cells at the lower levels have smaller reception fields than cells at the higher levels, and information aggregates from bottom to top [46], [21]. Higher layer networks, based on the segmentation results in the lower layer networks, are responsible for segmentation over larger scales.

Fig. 17 illustrates a two-layer image segmentation scheme. On the first layer, the image is decomposed into four disjoint parts. Each part is treated as an independent image where a basic image segmentation is performed (in this symbolic example, each part is segmented into two regions.) The second layer aggregates the segmentation results obtained on the first layer, using a single oscillator to represent each class segmented in the first layer, with the average gray level in the region as the oscillator input. The coupling connections on the second layer follow the topology of the regions on the first layer: second-layer oscillators whose underlying regions in the first layer are in vicinity are coupled. The segmentation on the second layer merges some regions obtained in the first layer and provides the final segmentation result. (In this example, regions A_2, B_2, C_2, and D_2 are merged on the second layer.) Fig. 18 presents a complete algorithm description. Multilayer segmentation can follow the same principle. From a computational point of view, the multilayer scheme saves memory and accelerates the program.

Multi-layer image segmentation.

1. First-layer image segmentation: decompose the image into P disjoint parts; each part is segmented in to M classes following the basic image segmentation algorithm in Fig. 10.

2. Second-layer segmentation.

   (a) Make the second-layer network with MP neural oscillators $\mathbf{x}_2(p, m)$, $p = 1, \ldots, P$, $m = 1, \ldots, M$ (see Step 1-(a) in Fig. 10). The oscillator $\mathbf{x}_2(p, m)$ represents class m in image part p in the first layer. The external input $I_{p,m} = a\left(\frac{\sum_{(i,j)\in\mathcal{C}_{p,m}} u_{i,j}}{|\mathcal{C}_{p,m}|}\right)$ is the average gray level of class m in image part p projected to the appropriate range (see Step 1 in Fig. 10).

   (b) Couple the second-layer oscillators with diffusive connections (3). The coupling strength is adapted from (9):

   $$k_{(p,m),(p',m')} = \begin{cases} e^{\frac{-|I_{p,m}-I_{p',m'}|^2}{\beta^2}} & \text{if } d_{\min}(\mathcal{C}_{p,m}, \mathcal{C}_{p',m'}) = 1 \\ 0 & \text{otherwise} \end{cases},$$

   where $d_{\min}(\mathcal{C}_{p,m}, \mathcal{C}_{p',m'})$ is the spatial Euclidean distance between the closest points in the classes $\mathcal{C}_{p,m}$ and $\mathcal{C}_{p',m'}$ and β value follows Step 1-(a) in the basic image segmentation algorithm in Fig. 10.

   (c) Segment the second-layer oscillators constructed in Steps 2(a) and 2(b) in M classes. The segmentation procedure follows Steps 2 and 3 in the basic image segmentation algorithm in Fig. 10.

3. Assign each pixel in the image to a class obtained in Step 2. (i_x, i_y), segmented in class m in image part p in the first layer, is assigned to class $\lambda = 1, \ldots, M$ in the second layer if $\mathbf{x}_2(p, m)$ is segmented to class λ in the second layer.

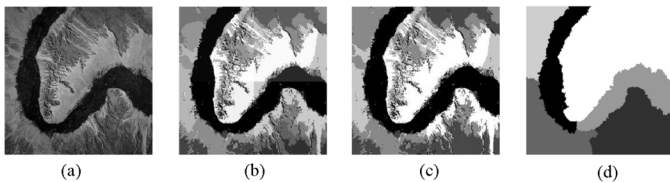Fig. 18. Complete algorithm description: multilayer image segmentation.

Fig. 19. (a) Aerial image (256×256). (b) and (c) Image segmentation by multilayer neural oscillators. (b) Segmentation result of the first layer ($\beta = 20, w = 3$). Each of the four 128×128 parts is segmented in six classes. (c) Segmentation result in six classes with the second layer ($\beta = 20$). (d) Segmentation result of multiscale normalized cuts. The number of classes is six for all the methods.

Fig. 19 illustrates an example of two-layer image segmentation. The image of size 256×256 shown in Fig. 19(a) is decomposed into four 128×128 parts. Fig. 19(b) and (c) presents, respectively, the segmentation results of the first and second layers, both with six classes. From the first layer to the second, some regions are merged, which corrects some oversegmentation and eliminates some boundary artifacts in the first layer. The segmentation result in Fig. 19(c) is satisfactory. The river, although rather noisy in the original image, is segmented from the land with accurate and regular boundary. The two aspects

of the land are nicely segregated as well. The multiscale normalized cuts segmentation [8] with the same number of classes shown in Fig. 19(d) is less delicate. While the land is segregated into coarse regions with some important details missing, the river is oversegmented into two parts. Some river bank is confused with the river, which results in the zigzag effect along the border of the river.

Fig. 20 shows the two-layer neural oscillators segmentation on some Berkeley benchmark images (481×321) [36], in comparison with the multiscale normalized cuts [8] and the human segmentation results. While both neural oscillators and normalized cuts achieve rather satisfactory segmentation, with the same number of classes, the former seems to represent better important detail structures and more pertinent to human performance.

To segment an image of size 128×128, the basic neural oscillator solution implemented with Matlab on a Pentium 4 PC takes between 10 and 30 min. The extra complexity due to the feedback and the second layer in the multilayer setting is marginal since the second-layer network is very small. Compared to popular image segmentation algorithms such as normalized cuts [8], [48], the neural oscillator approach has a higher computational cost as it involves solving differential equations (although this may make it extend more naturally to time-varying images).
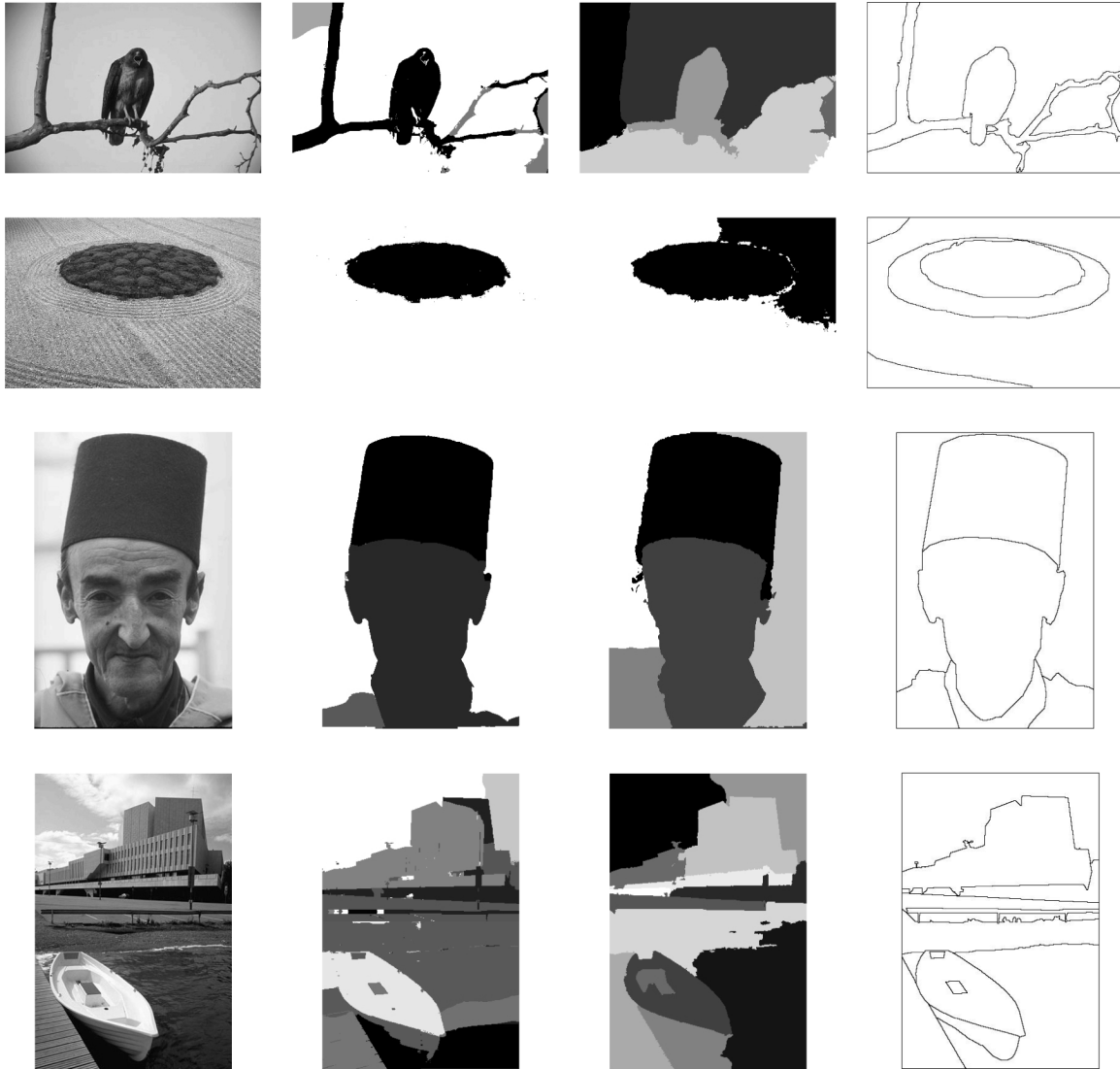
Fig. 20. Segmentation on the Berkeley data set. First column: images to segment. Second and third columns: segmentation results of two-layer neural oscillators ($\beta = 20, w = 3$) and normalized cuts (from top to bottom, respectively, 6, 2, 5, and 13 classes). Fourth column: human segmentation results.

The multilayer strategy provides an option to reduce computational time, since solving the smaller scale networks in the first layer is faster and in addition can be implemented in parallel.

VI. Concluding Remarks

Inspired by neural synchronization mechanisms in perceptual grouping, simple networks of neural oscillators coupled with diffusive connections have been proposed to implement visual grouping problems. Stable multilayer algorithms and feedback mechanisms have also been studied. Compared with state-of-the-art approaches, the same algorithm has been shown to achieve promising results on several classical visual grouping problems, including point clustering, contour integration, and image segmentation. As in any algorithm based on the simulation of a large network of dynamical systems, our visual grouping algorithm by neural oscillators has a relatively high computational complexity. Implementation with parallel computing systems such as very large scale integration (VLSI)

or graphic processing unit (GPU) will be useful for extensive acceleration [17].

Appendix
Convergence and Stability

One can verify ([44], to which the reader is referred for more details on the analysis tools) that a sufficient condition for global exponential concurrent synchronization of an oscillator network is

$$\lambda_{\min}(\mathbf{VLV}^T) > \sup_{\mathbf{a},t} \lambda_{\max}\left(\frac{\partial \mathbf{f}}{\partial \mathbf{x}}(\mathbf{a}, t)\right) \tag{10}$$

where $\lambda_{\min}(\mathbf{A})$ and $\lambda_{\max}(\mathbf{A})$ are, respectively, the smallest and largest eigenvalues of the symmetric matrix $\mathbf{A}_s = (\mathbf{A} + \mathbf{A}^T)/2$, $\mathbf{L}$ is the Laplacian matrix of the network ($\mathbf{L}_{ii} = \sum_{j \neq i} k_{ij}, \mathbf{L}_{ij} = -k_{ij}$ for $j \neq i$), and $\mathbf{V}$ is a projection matrix on $\mathcal{M}^\perp$. Here $\mathcal{M}^\perp$ is the subspace orthogonal to the

subspace $\mathcal{M}$ in which *all* the oscillators are in synchrony—or, more generally, in the case of a hierarchy, where all oscillators at each level of the hierarchy are in synchrony (i.e., $\mathbf{x}_1 = \cdots = \mathbf{x}_N$ at each level). Note that $\mathcal{M}$ itself need not be invariant (i.e., all oscillators synchronized at each level of the hierarchy need not be a particular solution of the system), but only needs to be a *subspace* of the actual invariant synchronization subspace [19], [44, Sec. 3.3.i.]), which may consist of synchronized subgroups according to the input image. Indeed, the space where all $\mathbf{x}_i$ are equal (or, in the case of a hierarchy, where at each level all $\mathbf{x}_i$ are equal), while in general not invariant, is always a subspace of the actual invariant subspace corresponding to synchronized subgroups.

These results can be applied, e.g., to individual oscillator dynamics of the type (1). Let $\mathbf{J_i}$ denote the Jacobian matrix of the individual oscillator dynamics (1), $\mathbf{J_i} = \partial[\dot{v}_i \; \dot{w}_i]^T / \partial[v_i, w_i]^T$. Using a diagonal metric transformation $\mathbf{\Theta} = \mathrm{diag}(\sqrt{c\alpha\beta}, 1)$, one easily shows, similarly to [58] and [59], that the transformed Jacobian matrix $\mathbf{\Theta}\mathbf{J_i}\mathbf{\Theta}^{-1} - \mathrm{diag}(k, 0)$ is negative definite for $k > 3 + (\alpha\beta)/(4)$. More general forms of oscillators can also be used. For instance, other second-order models can be created based on a smooth function $f(\cdot)$ and an arbitrary sigmoid-like function $\sigma(\cdot) \geq 0$ such that $0 \leq \sigma'(\cdot) \leq 1$, in the form

$$\dot{v}_i = f(v_i) - w_i + I_i \tag{11}$$

$$\dot{w}_i = c[\alpha\sigma(\beta v_i) - w_i] \tag{12}$$

with the transformed Jacobian matrix negative definite for $k > f'(v_i) + (\alpha\beta)/(4)$.

From a stability analysis point of view, the coupling matrix $\mathbf{K}$ of the Gaussian-tuned coupling, composed of coupling coefficients k_{ij} in (4), presents desirable properties. It is symmetric, and the classical theorem of Schoenberg (see [38]) shows that it is positive definite. Also, although it may actually be state dependent, the coupling matrix $\mathbf{K}$ can always be treated simply as a time-varying external variable for stability analysis and Jacobian computation purposes, as detailed in [58, Sec. 4.4], and [44, Sec. 2.3].

ACKNOWLEDGMENT

REFERENCES

[1] G. Aubert and P. Kornprobst, *Mathematical Problems in Image Processing: Partial Differential Equations and the Calculus of Variations*, 2nd ed. New York: Springer-Verlag, 2006.

[2] G. J. Brown and D. L. Wang, "Modelling the perceptual segregation of double vowels with a network of neural oscillators," *Neural Netw.*, vol. 10, no. 9, pp. 1547–1558, 1997.

[3] A. Buades, B. Coll, and J. M. Morel, "A review of image denoising algorithms, with a new one," *Multiscale Model. Simul.*, vol. 4, no. 2, pp. 490–530, 2005.

[4] G. Buzsaki, *Rhythms of the Brain*. New York: Oxford Univ. Press, 2006.

[5] K. Chen and D. L. Wang, "A dynamically coupled neural oscillator network for image segmentation," *Neural Netw.*, vol. 15, no. 3, pp. 423–439, 2002.

[6] Y. Cheng, "Mean shift, mode seeking, and clustering," *IEEE Trans. Pattern Anal. Mach. Intell.*, vol. 17, no. 8, pp. 790–799, Aug. 1995.

[7] D. Comaniciu and P. Meer, "Mean shift: A robust approach toward feature space analysis," *IEEE Trans. Pattern Anal. Mach. Intell.*, vol. 24, no. 5, pp. 603–619, May 2002.

[8] T. B. Cour, F. Benezit, and J. Shi, "Spectral segmentation with multiscale graph decomposition," in *Proc. IEEE Comput. Soc. Conf. Comput. Vis. Pattern Recognit.*, 2005, vol. 2, pp. 1124–1131.

[9] A. Desolneux, L. Moisan, and J.-M. Morel, "Computational gestalts and perception thresholds," *J. Physiol. Paris*, vol. 97, no. 2–3, pp. 311–322, 2003.

[10] A. Desolneux, L. Moisan, and J.-M. Morel, "A grouping principle and four applications," *IEEE Trans. Pattern Anal. Mach. Intell.*, vol. 25, no. 4, pp. 508–513, Apr. 2003.

[11] A. Desolneux, L. Moisan, and J.-M. Morel, *Gestalt Theory and Image Analysis, A Probabilistic Approach*, ser. Interdisciplinary Applied Mathematics. New York: Springer-Verlag, 2007 [Online]. Available: http://www.cmla.enscachan.fr/Utilisateurs/morel/lecturenote.pdf

[12] F. Cao, J. Delon, A. Desolneux, P. Musé, and F. Sur, "A unified framework for detecting groups and application to shape recognition," *J. Math. Imag. Vis.*, vol. 27, no. 2, pp. 91–119, 2007.

[13] O. Faugeras, F. Grimbert, and J. J. Slotine, "Stability and synchronization in neural fields," *SIAM J. Appl. Math.*, vol. 68, no. 1, pp. 205–250, 2008.

[14] D. J. Field, A. Hayes, and R. F. Hess, "Contour integration by the human visual system: Evidence for a local "association field"," *Vis. Res.*, vol. 33, no. 2, pp. 173–193, Jan. 1993.

[15] R. FitzHugh, "Impulses and physiological states in theoretical models of nerve membrane," *Biophys. J.*, vol. 1, pp. 445–466, 1961.

[16] K. Fukunaga and L. Hostetler, "The estimation of the gradient of a density function, with applications in pattern recognition," *IEEE Trans. Inf. Theory*, vol. IT-21, no. 1, pp. 32–40, Jan. 1975.

[17] D. Geiger and F. Girosi, "Parallel and deterministic algorithms from MRFs: Surface reconstruction," *IEEE Trans. Pattern Anal. Mach. Intell.*, vol. 13, no. 5, pp. 401–412, May 1991.

[18] S. Geman and D. Geman, "Stochastic relaxation, Gibbs distributions, and the Bayesian restoration of images," *IEEE Trans. Pattern Anal. Mach. Intell.*, vol. 6, no. PAMI-6, pp. 721–741, Nov. 1984.

[19] L. Gerard and J. J. E. Slotine, "Neuronal networks and controlled symmetries," [Online]. Available: arXiv:q-bio/0612049v4

[20] L. Grady, "Space-variant computer vision: A graph-theoretic approach," Ph.D. dissertation, Grad. Schl. Arts Sci., Boston Univ., Boston, MA, 2004.

[21] J. Hawkins and S. Blakeslee, *On Intelligence*. New York: Holt, 2005.

[22] R. F. Hess, A. Hayes, and D. J. Field, "Contour integration and cortical processing," *J. Physiol. Paris*, vol. 97, no. 2–3, pp. 105–119, 2003.

[23] E. R. Kandel, J. J. Schwartz, and T. M. Jessel, *Principles of Neural Science*, 4th ed. New York: McGraw-Hill, 2000.

[24] G. Kanizsa, *Traduction Française: La Grammaire du Voir*. Paris, France: Diderot Editeur, Arts et Sciences, 1996.

[25] M. Kuzmina, E. Manykin, and I. Surina, "Tunable oscillatory network for visual image segmentation," in *Proc. Int. Conf. Artif. Neural Netw.*, 2001, pp. 1013–1019.

[26] M. Kuzmina, E. Manykin, and I. Surina, "Oscillatory network with self-organized dynamical connections for synchronization-based image segmentation," *BioSystems*, vol. 76, no. 1–3, pp. 43–53, 2004.

[27] T. S. Lee, "Computations in the early visual cortex," *J. Physiol. Paris*, vol. 97, no. 2–3, pp. 121–139, 2003.

[28] Z. Li, "A neural model of contour integration in the primary visual cortex," *Neural Comput.*, vol. 10, no. 4, pp. 903–940, 1998.

[29] Z. Li, "Visual segmentation by contextual influences via intra-cortical interactions in the primary visual cortex," *Network, Comput. Neural Syst.*, vol. 10, no. 2, pp. 187–212, 1999.

[30] Z. Li, "Pre-attentive segmentation in the primary visual cortex," *Spatial Vis.*, vol. 13, no. 1, pp. 25–50, 2000.

[31] Z. Li, "Computational design and nonlinear dynamics of a recurrent network model of the primary visual cortex*," *Neural Comput.*, vol. 13, no. 8, pp. 1749–1780, 2001.

[32] X. Liu and D. L. Wang, "Range image segmentation using a relaxation oscillator network," *IEEE Trans. Neural Netw.*, vol. 10, no. 3, pp. 564–573, May 1999.

[33] X. Liu and D. L. Wang, "A spectral histogram model for texton modeling and texture discrimination," *Vis. Res.*, vol. 42, no. 23, pp. 2617–2634, 2002.

[34] X. Liu and D. L. Wang, "Image and texture segmentation using local spectral histograms," *IEEE Trans. Image Process.*, vol. 15, no. 10, pp. 3066–3077, Oct. 2006.

[35] S. Mallat, "Geometrical grouplets," *Appl. Comput. Harmonic Anal.*, vol. 26, no. 2, pp. 161–180, 2008.

[36] D. Martin, C. Fowlkes, D. Tal, and J. Malik, "A database of human segmented natural images and its application to evaluating segmentation algorithms and measuring ecological statistics," in *Proc. 8th Int. Conf. Comput. Vis.*, Jul. 2001, vol. 2, pp. 416–423.

[37] W. Metzger, *Laws of Seeing*. Cambridge, MA: MIT Press, 2006.

[38] C. A. Micchelli, "Interpolation of scattered data: Distance matrices and conditionally positive definite functions," *Constructive Approx.*, vol. 2, pp. 11–22, 1986.

[39] J. M. Morel and S. Solimini, "Variational methods in image segmentation," in *Progress in Nonlinear Differential Equations and Their Applications*. Berlin, Germany: Birkhauser-Verlag, 1995, vol. 14.

[40] D. Mumford and J. Shah, "Optimal approximations by piecewise smooth functions and associated variational problems," *Commun. Pure Appl. Math*, vol. 42, no. 5, pp. 577–685, 1989.

[41] J. Nagumo, S. Arimoto, and S. Yoshizawa, "An active pulse transmission line simulating nerve axon," *Proc. IRE*, vol. 50, no. 10, pp. 2061–2070, Oct. 1962.

[42] E. Olson, M. Walter, J. Leonard, and S. Teller, "Single cluster graph partitioning for robotics applications," *Proc. Robot. Sci. Syst.*, pp. 265–272, 2005.

[43] P. Perona and W. Freeman, "A factorization approach to grouping," in *Proc. Eur. Conf. Comput. Vis.*, 1998, vol. 1, pp. 655–670.

[44] Q. C. Pham and J. J. Slotine, "Stable concurrent synchronization in dynamic system networks," *Neural Netw.*, vol. 20, no. 1, pp. 62–77, 2007.

[45] U. Polat and D. Sagi, "Lateral interactions between spatial channels: Suppression and facilitation revealed by lateral masking experiments," *Vis. Res.*, vol. 33, pp. 993–999, 1992.

[46] R. P. N. Rao and D. H. Ballard, "Predictive coding in the visual cortex: A functional interpretation of some extra-classical receptive-field effects," *Nature Neurosci.*, vol. 2, pp. 79–87, 1999.

[47] T. Serre, L. Wolf, S. Bileschi, M. Riesenhuber, and T. Poggio, "Robust object recognition with cortex-like mechanisms," *IEEE Trans. Pattern Anal. Mach. Intell.*, vol. 29, no. 3, pp. 411–426, Mar. 2007.

[48] J. Shi and J. Malik, "Normalized cuts and image segmentation," *IEEE Trans. Pattern Anal. Mach. Intell.*, vol. 22, no. 8, pp. 888–905, Aug. 2000.

[49] W. Singer and C. M. Gray, "Visual feature integration and the temporal correlation hypothesis," *Annu. Rev. Neurosci.*, vol. 18, no. 1, pp. 555–586, 1995.

[50] E. Sudderth and M. I. Jordan, "Shared segmentation of natural scenes using dependent Pitman-Yor processes," in *Advances in Neural Information Processing Systems*. Cambridge, MA: MIT Press, 2009, vol. 21.

[51] D. Terman and D. L. Wang, "Global competition and local cooperation in a network of neural oscillators," *Physica D: Nonlinear Phenomena*, vol. 81, no. 1–2, pp. 148–176, 1995.

[52] S. Ullman and A. Shashua, "Structural saliency: The detection of globally salient structures using a locally connected network," in *Proc. Int. Conf. Comput. Vis.*, Clearwater, FL, 1988, pp. 321–327.

[53] D. L. Wang, "The time dimension for scene analysis," *IEEE Trans. Neural Netw.*, vol. 16, no. 6, pp. 1401–1426, Nov. 2005.

[54] D. L. Wang and G. J. Brown, "Separation of speech from interfering sounds based on oscillatory correlation," *IEEE Trans. Neural Netw.*, vol. 10, no. 3, pp. 684–697, May 1999.

[55] D. L. Wang and P. Chang, "An oscillatory correlation model of auditory streaming," *Cogn. Neurodyn.*, vol. 2, no. 1, pp. 7–19, 2008.

[56] D. L. Wang and D. Terman, "Locally excitatory globally inhibitory oscillator networks," *IEEE Trans. Neural Netw.*, vol. 6, no. 1, pp. 283–286, Jan. 1995.

[57] D. L. Wang and D. Terman, "Image segmentation based on oscillatory correlation," *Neural Comput.*, vol. 9, no. 4, pp. 805–836, 1997.

[58] W. Wang and J. J. E. Slotine, "On partial contraction analysis for coupled nonlinear oscillators," *Biol. Cybern.*, vol. 92, no. 1, pp. 38–53, 2005.

[59] W. Wang and J. J. E. Slotine, "Contraction analysis of time-delayed communications and group cooperation," *IEEE Trans. Autom. Control*, vol. 51, no. 4, pp. 712–717, Apr. 2006.

[60] R. J. Watt and W. A. Phillips, "The function of dynamic grouping in vision," *Trends Cogn. Sci.*, vol. 4, no. 12, pp. 447–454, 2000.

[61] M. Wertheimer, "Laws of organization in perceptual forms," in *A Source Book of Gestalt Psychology*, W. Ellis, Ed. London, U.K.: Routledge & Kegan Paul, 1938, pp. 71–88.

[62] S. C. Yen and L. H. Finkel, "Extraction of perceptually salient contours by striate cortical networks," *Vis. Res.*, vol. 38, no. 5, pp. 719–741, 1998.
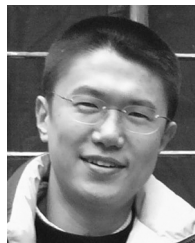
Guoshen Yu received the B.Sc. degree in electronic engineering from Fudan University, Shanghai, China, in 2003, the engineering degree from Télécom ParisTech, Paris, France, in 2006, the M.Sc. degree in applied mathematics from ENS de Cachan, Cachan, France, in 2006, and the Ph.D. degree in applied mathematics from Ecole Polytechnique, Palaiseau, France, in 2009.

He is now a Postdoctoral Research Associate at the Electrical and Computer Engineering Department, University of Minnesota, Twin Cities. He was a research intern with STMicroelectronics, Agrate, Italy, and with Let It Wave, Paris, France, for one year in 2005–2006. In spring 2008 semester, he was a visiting graduate student in the Mechanical Engineering Department, Massachusetts Institute of Technology (MIT), Cambridge. His research interests include signal, image, and video processing and computer vision.

Dr. Yu received the Gaspard Monge International Doctoral Grant from Ecole Polytechnique from 2006 to 2008.

Jean-Jacques Slotine was born in Paris, France, in 1959. He received the Ph.D. degree in aeronautics and astronautics from the Massachusetts Institute of Technology (MIT), Cambridge, in 1983.

After working at Bell Labs in the Computer Research Department, in 1984, he joined the faculty at MIT, where he is now Professor of Mechanical Engineering and Information Sciences, Professor of Brain and Cognitive Sciences, and Director of the Nonlinear Systems Laboratory (NSL). He is the coauthor of the textbooks *Robot Analysis and Control* (New York: Wiley, 1986) and *Applied Nonlinear Control* (Englewood Cliffs, NJ: Prentice-Hall, 1991).

Prof. Slotine was a member of the French National Science Council from 1997 to 2002, and is a member of Singapore's A*STAR SigN Advisory Board.